# Crystal growth and spectroscopic characterization of $Tm^{3+}$-doped $KYb(WO_4)_2$ single crystals

M. C. Pujol, F. Güell, X. Mateos, Jna. Gavaldà, R. Solé, J. Massons, M. Aguiló, and F. Díaz*
*Laboratori de Física i Cristal·lografia de Materials (FiCMA) and IEA, Universitat Rovira i Virgili, 43005 Tarragona, Spain*

G. Boulon and A. Brenier
*Physico Chimie des Matériaux Luminescents, Université Claude Bernard Lyon, 69622 Villeurbanne Cedex, France*
(Received 25 April 2002; published 16 October 2002)

In this paper we present the crystal growth and optical characterization of thulium-doped $KYb(WO_4)_2$ (hereafter KYbW). We grew thulium-doped KYbW monoclinic single crystals with optimal crystalline quality by the top-seeded-solution-growth (TSSG) slow-cooling method. Thulium spectroscopy was characterized in this host. The Judd-Ofelt parameters determined were $\Omega_2=0.14\times10^{-20}$ cm$^2$, $\Omega_4=0.21\times10^{-20}$ cm$^2$, and $\Omega_6=0.10\times10^{-20}$ cm$^2$. The room temperature lifetimes measured for KYbW:Tm 1% were $\tau(^1G_4)=60$–$70$ $\mu$s, $\tau(^3H_4)=90$ $\mu$s and $\tau(^3F_4)=200$ $\mu$s. We calculated the emission cross section for several channels. There was an important blue emission after pumping resonantly to the stoichiometric ytterbium at 980 nm, and we studied the emission channels of thulium. The presence of thulium luminescence is proof of the large transfer of energy in this compound.

DOI: 10.1103/PhysRevB.66.144304 PACS number(s): 78.20.−e, 78.55.−m, 42.55.−f, 81.10.−h

## I. INTRODUCTION

The monoclinic phases of the double potassium rare-earth tungstates $[KRE(WO_4)_2$, $R=$Gd and Y] are well known hosts that are an interesting area of research into rare-earth-doped solid-state lasers. KYbW crystals belong to this family of tungstates. Their special feature is that they form an ytterbium stoichiometric material.

Ytterbium ions have several advantages. They have a high absorption cross section and broad band absorption in the 900–1000 nm (11 111–10 000 cm$^{-1}$) spectral range, which is suitable for the laser diodes. Energy transfer from ytterbium to another lanthanide such as erbium, thulium, holmium, neodymium, etc., is efficient, which means that these others ions can be excited indirectly to receive luminescence from them. Lanthanide doping of this crystalline host offers several interesting applications with the stoichiometric ytterbium used as sensitizer.

The aim of this paper is to develop a diode-pumped laser source that operates at visible and IR ranges and is based on thulium emissions sensitised by ytterbium. To our knowledge, this is the first time that $Tm^{3+}$ spectroscopy has been studied in this host. The usual laser transitions of thulium are infrared emission at 1.8 $\mu$m ($^3F_4\rightarrow{}^3H_6$ transition, energy $\cong$5900–5000 cm$^{-1}$, $\lambda\cong1.7$–$2$ $\mu$m), which has applications in medicine and remote sensing, and blue visible emission at 450 nm ($^1D_2\rightarrow{}^3F_4$ transition, energy $\cong$22 727–21 275 cm$^{-1}$, $\lambda\cong$440–470 nm).[1] Thulium transition at 1.5 $\mu$m ($^3H_4\rightarrow{}^3F_4$ transition, energy $\cong$6760–6475 cm$^{-1}$, $\lambda\cong1.48$–$1.54$ $\mu$m) is also interesting because of its eye-safe region and optical communications due to the third optical transmission window of the silica fibers. Laser action at 1.5 $\mu$m of thulium ion has been realised by sensitization with Yb in YLF fibres after excitation by diode and YAG:$Nd^{3+}$ pumping.[2–4]

$Tm^{3+}$ can be directly excited into its $^3H_4$ emitting level with high power and well-developed GaAlAs laser diodes around 800 nm. The thulium concentration must be high enough to ensure that pumping is efficient pump but low enough to minimize concentration quenching effects due to cross relaxation type ($^3H_4+{}^3H_6\rightarrow{}^3F_4+{}^3F_4$) and nonradiative energy transfer between active ions. However, in all crystalline materials the lifetime of the $^3F_4$ terminal level of the laser transition is longer than that of the $^3H_4$ emitting level. This creates a detrimental bottlenecking effect during the optical cycle. Codoping with a deactivator such as $Ho^{3+}$, $Yb^{3+}$, and $Tb^{3+}$ reduces the $^3F_4$ lifetime.[5]

The first report of continuous wave (CW) room-temperature laser operation of the 2 $\mu$m emission of $Tm^{3+}$, pumped by diode laser was in YAG:$Tm^{3+}$.[6] However, one problem with thulium is that it depends strongly on the pump diode temperature because of the relatively narrow Tm absorption bands in YAG and YLF. With tungstates, this laser emission was achieved in 1997 by Kaminskii *et al.*[7,8] in KGW:$Tm^{3+}$:$Er^{3+}$:$Yb^{3+}$ at 1.92 and 1.93 $\mu$m and in 2000 by Bagaev *et al.*[9] in KYW:Tm at 1.95 $\mu$m. The 2-micron laser is useful for spectroscopically sensing hydrocarbon gases that absorb around these wavelengths.[10] The main problem with this process is the up conversion via $^1G_4$ multiplet. A 2.3 $\mu$m laser action has already been achieved in compounds: YAG:Tm:Cr,[11] YAL:Tm, and Tm:Ho: YLF.

In this paper we present the growth of a $Tm^{3+}$-doped KYbW crystal and the determination of the energy position of 61 thulium sublevels taken from the polarized optical absorption at low temperature. We present the room-temperature optical absorption cross sections of the energy levels and use them to calculate the stimulated emission cross section of the 1.8 $\mu$m emission. We present the luminescence of thulium in KYbW at RT and 6 K and the lifetime measurements of the energy levels after ytterbium excitation. We used Judd-Ofelt theory[12,13] to calculate the theoretical lifetimes of the energy levels. Finally, we discuss the mechanisms of Yb-Tm energy transfer.

## II. CRYSTAL GROWTH

We grew KYbW: $Tm^{3+}$ single crystals by the top-seeded-solution-growth (TSSG) slow-cooling method using

 

TABLE I. Details of crystal growth. A: Temperature gradient in the solution, K/mm. B: $Tm_2O_3/(Yb_2O_3+Tm_2O_3)$ ratio in the solution, mol%. C: Seed orientation. D: Cooling rate, K/h. E: Cooling interval, K. F: Crystal weight, g. G: Growth rate ($\times 10^{-4}$), g/h. H: Macrodefects. I: Crystal dimensions along *c* direction, mm. J: Crystal dimensions along *a** direction, mm. K: Crystal dimensions along *b* direction, mm. L: Temperature of saturation K.

| A | B | C | D | E | F | G | H | I | J | K | L |
|---|---|---|---|---|---|---|---|---|---|---|---|
| 0.13 | 0.5% Tm | b | 0.1 | 10 | 2.83 | 283 | – | 16.00 | 8.3 | 5.35 | 1177.2 |
| 0.13 | 1% Tm | b | 0.1 | 17.2 | 3.95 | 230 | – | 15.74 | 9.97 | 6.62 | 1177.5 |
| 0.13 | 3% Tm | b | 0.1 | 15 | 3.92 | 261 | – | 15.18 | 10.03 | 7.25 | 1175.9 |
| 0.13 | 5% Tm | −b | 0.1 | 20 | 4.99 | 249 | – | 15.20 | 10.38 | 7.50 | 1176.3 |

$K_2W_2O_7$ solvent according to the method described elsewhere.[14,15] We carried out crystal growth experiments at 1175–1180 K as temperature of saturation with a ratio of 11.5% / 88.5% solute/solvent molar of the phase diagram. To obtain samples with different thulium concentrations, we fixed $Tm_2O_3/(Yb_2O_3+Tm_2O_3)$ molar ratios of ytterbium oxide substitution at 0.005, 0.01, 0.03, and 0.05. The crucible was placed in a vertical furnace such that the axial temperature gradient in the solution was about 1.3 K/cm (hot bottom), while the radial temperature gradient was about 1 K/cm (hot crucible wall).

After the solution homogenized, we determined the saturation temperature with a KYbW seed in contact with the free surface of the solution. We chose the crystallography *b* axis as the orientation of crystal growth to increase the growth rate and grow inclusion-free crystals, as we have previously described. We decreased the temperature of the solution at a rate of 0.1 K/h for about 10–20 K. Crystal rotation was at 40 rpm. After 8–10 days, we removed the crystals slowly from the solution and cooled them to RT at 15 K/h to prevent thermal shocks.

In summary, the dimensions of the crystals were typically 8.3–10.4 mm×5.3–7.5 mm×15.1–16 mm in the *a**, *b*, and *c* crystallographic directions, respectively. They each weighed about 2.8–5 g. Our crystal growth conditions allowed an average growth rate of 0.025–0.030 g/h. Table I shows the main information about crystal growth and Fig. 1 shows a photograph of a KYbW:Tm single crystal.

The composition of the single crystals was measured by EPMA with a Cameca Camebax SX 50 equipment. The distribution coefficient of the thulium in KYbW was determined by

$$K_{Ln^{3+}} = \frac{[\text{mole } Tm^{3+}/(\text{mole } Tm^{3+} + \text{mole } Yb^{3+})]_{\text{crystal}}}{[\text{mole } Tm^{3+}/(\text{mole } Tm^{3+} + \text{mole } Yb^{3+})]_{\text{solution}}}, \quad (1)$$

where $Ln^{3+}$ are trivalent thulium ions.

For the constitutional elements K, W, Yb, and O, we used undoped KYbW as standard reference. To measure thulium, we used the L$\alpha$ line and the REE2 standard. These measurements provide a distribution coefficient of $Tm^{3+}$ close to unity. This ensures the homogeneous distribution of thulium in KYbW, which is necessary for laser applications. Table II shows the EPMA results. For the spectroscopic characterization, we oriented the samples using their morphology and x-ray diffraction.

## III. THULIUM SPECTROSCOPY

### A. Absorption studies

We performed the polarized optical absorption of thulium at RT and at low temperature (6 K) using a Cary Varian 500 spectrophotometer. We cooled the sample for the 6 K experiments with a Leybold RDK-6-320 closed-cycle Helium cryostat.

The high anisotropy of our tungstates, makes it necessary to measure the optical absorption with polarized light parallel to the three principal directions of the crystal. The sample for our absorption experiments was a prism of $KYb_{0.993}Tm_{0.007}(WO_4)_2$ whose polished faces were parallel to the principal planes (optical quality) to ensure parallelism between the electrical field of the radiation and the principal optical axis. Figure 2 shows the polarized optical absorption of KYbW:$Tm^{3+}$ at RT in the 30 000–5000 $cm^{-1}$ (350–2000 nm) spectral range.

As well as the excited energy levels of thulium ion, the spectrum shows a broad band at about 10 000 $cm^{-1}$ (1000 nm) corresponding to $^2F_{7/2} \rightarrow {}^2F_{5/2}$ transition of $Yb^{3+}$. We

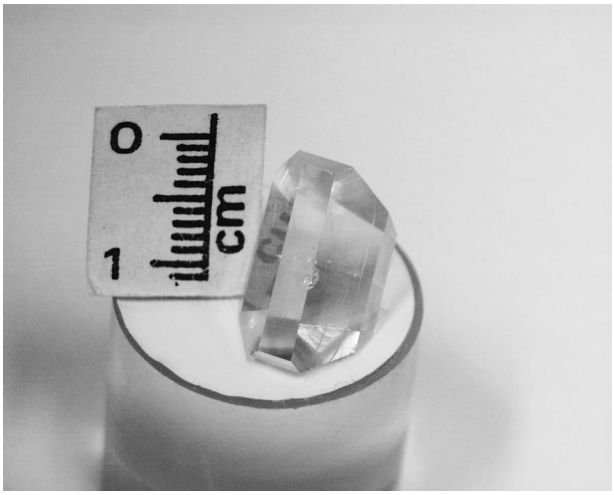


FIG. 1. Photograph of KYbW doped with thulium single crystal grown in the *b* direction.

TABLE II. Summary of the EPMA results of the analysis of KYbW:$Tm^{3+}$.

| | $K_{Ln}{}^{3+}$ | $[Tm^{3+}]$ (at.cm$^3$) | % Weight | Stoichiometric formula |
|---|---|---|---|---|
| 0.5% | 1.47 | $4.8\times10^{19}$ | $0.713\pm0.018$ | $KYb_{0.993}Tm_{0.007}(WO_4)_2$ |
| 1% | 1.23 | $7.95\times10^{19}$ | $1.161\pm0.019$ | $KYb_{0.988}Tm_{0.012}(WO_4)_2$ |
| 3% | 1.13 | $2.19\times10^{20}$ | $3.240\pm0.026$ | $KYb_{0.967}Tm_{0.033}(WO_4)_2$ |
| 5% | 1.07 | $3.47\times10^{20}$ | $5.214\pm0.034$ | $KYb_{0.947}Tm_{0.054}(WO_4)_2$ |

have already described spectroscopic characterization of the stoichiometric ytterbium in this host.[16]

The absorption cross section of the $^3H_4$ manifold of $Tm^{3+}$ was the broadest. For P polarization the most intense absorption was at 793.6 nm with an absorption cross section of $8.8\times10^{-20}$ cm$^2$ (band width 3.5 nm), while for polarization parallel to the $N_m$ at 801.8 nm, the absorption cross section was $4.8\times10^{-20}$ cm$^2$ (band width 1.4 nm). However, we increased the efficiency of the pump process by exciting $Tm^{3+}$ indirectly via energy transfer of ytterbium. This was because the ytterbium ion has a higher broad band in the $^2F_{5/2}$ energy level and a good absorption cross section to be excited. In this way we can choose the optimal $Tm^{3+}$ concentration to avoid phenomena such as nonradiative processes or Tm-Tm cross relaxation.

The splitting of thulium in KYbW was determined by 6 K optical absorption (Fig. 3). At low temperature, the thermal population of the sublevels of the ground state and any vibronic transition (electron-phonon coupling) were minimized. To understand the energetic sublevels better, we studied the thermal evolution of the optical absorption of the $^1G_4$ and $^3H_4$ energy levels (Fig. 4). There were contributions from thermally populated excited levels (117, 136, and 254 cm$^{-1}$) of $^3H_6$ multiplet at 80 K.

Table III shows around 61 energetic positions of the sublevels of the $Tm^{3+}$ energy levels determined in the above spectral range. These energetic positions agree with those in the literature for other hosts[17,18] and their multiplicity are as expected, if we assume only one center for the thulium ion with $C_2$ symmetry.

We can use the Judd-Ofelt[10,11] theory to describe the radiative optical properties of lanthanide. This is a second-order approximation for studying lanthanide one-photon $f$-$f$ transition.

We used the matrix elements given by Weber *et al.* in the calculation.[19] We treated the contributions of each polarization configuration separately and calculated the $\Omega_k^{g,p,m}$ set by minimizing the differences between the measured and the theoretical oscillator strengths by $\Sigma_{J'}(f_{\exp}-f_{ED,th})^2$. We cal-

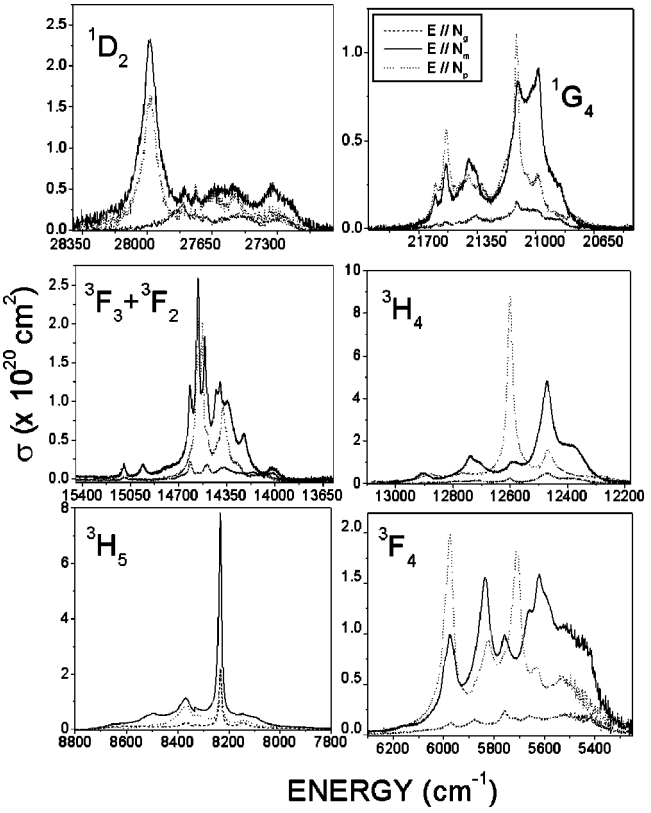


FIG. 2. Polarized room-temperature optical absorption of KYbW doped with thulium.

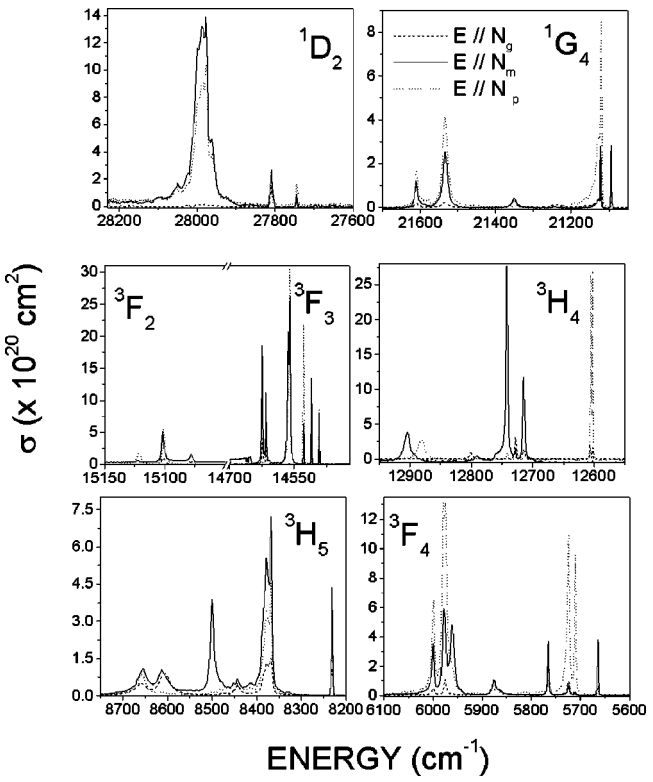


FIG. 3. Polarized low-temperature absorption of KYbW doped with thulium.

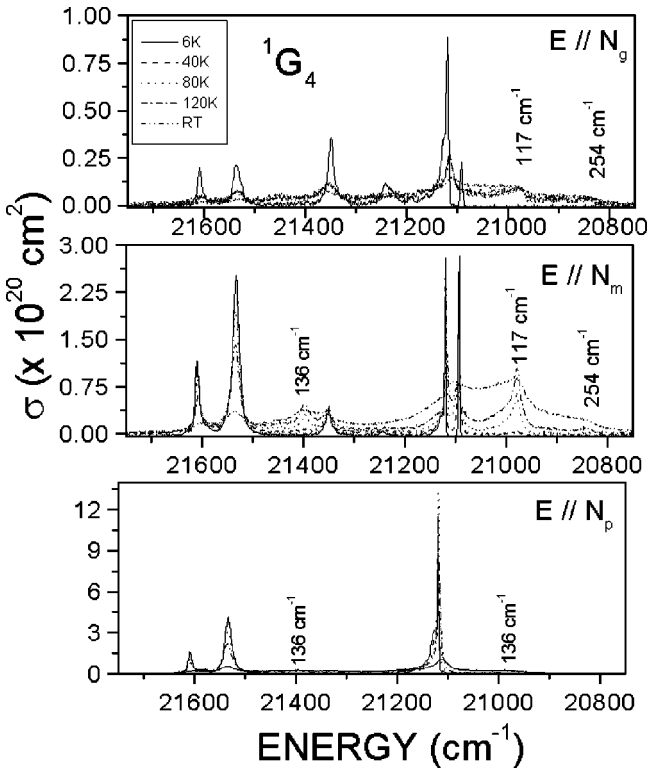


FIG. 4. Evolution with temperature of the optical absorption of the $^1G_4$ multiplet.

culated the $f_{ED,th}$ value of each $JJ'$ multiplet with the corresponding refractive indices $n_g$, $n_m$, and $n_p$ of the KYbW matrix at the corresponding $\bar{\lambda}$ of the multiplet ($n$ is the refractive index of the medium, calculated using the Sellmeier coefficients of KYbW host).[16] The JO parameters can be used to calculate the radiative transition rates, the radiative lifetime and the luminescence branching ratios of each transition.

As we were unable to separate the room temperature optical absorption of some multiplets, we treated these multiplets as a single set for the JO calculations. The quality of each fit is characterized by the root-mean-square (rms) deviations of the least-squares fitting.

Table IV shows the $\Omega_k$ values obtained and rms for every optical direction. Table V shows the radiative transition rates, radiative lifetimes and branching ratios of thulium in KYbW.

### B. Emission spectra studies

We measured the room-temperature and low-temperature fluorescence spectra with 90° geometry and excited with infrared radiation at 940 (10 638 cm$^{-1}$) using a narrow line width OPO BMI pulsed with the third harmonic of a BMI Saga 1.2 J Nd:YAG laser. Pump energy was about 10 mJ, with a pulse duration of 7 ns and a pulse repetition rate of 10 Hz. Fluorescence was dispersed by a 0.46 m focal length Jobin Yvon monochromator and captured by a R928 Hamamatsu PMT for the visible range and a R5509-72 Hamamatsu NIR PMT in the NIR range. The electronic signal was analyzed by a EG&G 7265 DSP lock-in amplifier. Samples for the low-temperature experiments were cooled as for absorption.

TABLE III. Energetic sublevels (cm$^{-1}$) of $Tm^{3+}$ observed at 6 K in the host $KYb(WO_4)_2$. Following the symmetry rules, the peaks belonging to M and G are the same, and P different. We indicated by ( ) the peaks that are not expected by symmetry, but they also appear.

| $^{2s+1}L_J$ | *Pol* | Energy (cm$^{-1}$) | $^{2s+1}L_J$ | *Pol* | Energy (cm$^{-1}$) |
|---|---|---|---|---|---|
| $^3H_6$ | | 0 | $^3H_4$ | $(G)P$ | 12 602 |
| One peak missing | | 95 | | $(G)P$ | 12606 |
| | | 107 | | $GM$ | 12 714 |
| | | 117 | | $GM$ | 12 728 |
| | | 136 | | $M(P)$ | 12 741 |
| | | 152 | | $M$ | 12 790 |
| | | 183 | | $G$ | 12 801 |
| | | 227 | | $P$ | 12 881 |
| | | 254 | | $M$ | 12 905 |
| | | 279 | | | |
| | | 346 | $^3F_3$ | $(GM)P$ | 14 491 |
| | | 517 | One peak missing | $GM$ | 14 510 |
| | | | | $(GM)P$ | 14 528 |
| $^3F_4$ | $GM(P)$ | 5664 | | $(GM)P$ | 14 559 |
| | $(GM)P$ | 5711 | | $GM$ | 14 615 |
| | $(GM)P$ | 5724 | | $GM$ | 14 623 |
| | $GM(P)$ | 5765 | | | |
| | $GM$ | 5864 | $^3F_2$ | $GM(P)$ | 15 078 |
| | $GM$ | 5875 | Two peaks missing | $(GM)P$ | 15 101 |
| | $M(P)$ | 5960 | | $(M)P$ | 15 122 |
| | $(GM)P$ | 5977 | | | |
| | $(GM)P$ | 6000 | $^1G_4$ | $GM$ | 21 094 |
| | | | One peak missing | $(GM)P$ | 21 121 |
| $^3H_5$ | $GM(P)$ | 8231 | | $(GM)P$ | 21 131 |
| Two peaks missing | $GM(P)$ | 8368 | | $GM$ | 21 245 |
| | $GM(P)$ | 8378 | | $GM$ | 21 350 |
| | $(M)P$ | 8413 | | $(GM)P$ | 21 534 |
| | $(GM)P$ | 8443 | | $P$ | 21 578 |
| | $P$ | 8480 | | $(GM)P$ | 21 610 |
| | $M$ | 8500 | | | |
| | $GM$ | 8610 | $^1D_2$ | $(GM)P$ | 27 745 |
| | $(GM)P$ | 8659 | | $GM(P)$ | 27 810 |
| | | | | $(M)P$ | 27 976 |
| | | | | $(M)P$ | 27 988 |
| | | | | $(M)P$ | 28 051 |

Figure 5 shows the room-temperature emission channels of KYbW:Tm. The emissions bands correspond well with those reported for $Tm^{3+}$ in other crystalline lattices. Under infrared pumping at 975 nm, KYbW:Tm 1% had nine emission channels (see Table VI). All these emission bands were from thulium ions excited by successive energy transfer after

TABLE IV. Phenomenologic parameter of Judd-Ofelt of $Tm^{3+}$ inside KYbW.

| | $\Omega_2\times10^{20}(cm^2)$ | $\Omega_4\times10^{20}(cm^2)$ | $\Omega_6\times10^{20}(cm^2)$ | rms($\Delta f$) |
|---|---|---|---|---|
| *G* | 0.04 | 0.07 | 0.09 | 3.2% |
| *M* | 0.27 | 0.25 | 0.11 | 11.7% |
| *P* | 0.12 | 0.32 | 0.09 | 16.4% |
| Unpolarized | 0.14 | 0.21 | 0.10 | 10.4% |

pumping $^2F_{5/2}$ multiplet of $Yb^{3+}$. We therefore had a large energy transfer in the KYbW material. Overall intensity emission was larger in the second blue channel $^1G_4\rightarrow{}^3H_6$ and in the far red 800 nm channel $^3H_4\rightarrow{}^3H_6$. The low intensity of the red channel ($^1G_4\rightarrow{}^3F_4$) was due to a repopulation of this manifold via cross-relaxation $^3H_4$, $^3H_6\rightarrow{}^3F_4$, $^3F_4$.[20]

There was also a strong concentration quenching in the channel $^1G_4\rightarrow{}^3H_6$, which is similar to the behavior of some codoped Tm,Yb crystals,[21] which was also due to cross relaxation between thulium ions.

Figure 6 shows the 6 K optical luminescence of the blue and the far-red channels, after pumping at 10 640 $cm^{-1}$ (940 nm) also via excitation of the ytterbium ion. We deduced energies of the Stark sublevels of the ground $^3H_6$ multiplet of $Tm^{3+}$ and included them in Table III.

We used the reciprocity method[22] to calculate the stimulated emission cross section of the $^3F_4\rightarrow{}^3H_6$ transition of thulium, with the RT absorption cross section line shape and the splitting determined at 6 K. We used the following equation:

$$\sigma_e(\upsilon)=\sigma_{\mathrm{abs}}(\upsilon)\frac{Z_l}{Z_u}\exp\left[\frac{(E_{zl}-h\upsilon)}{kT}\right], \tag{2}$$

where $Z_l$ and $Z_u$ are the partition functions of the ground energy level (lower) and excited energy level (upper), respectively, and $E_{zl}$ is the zero-line energy between the low-

TABLE V. Radiative transition rates, branching ratios and radiative lifetimes of $Tm^{3+}$ inside KYbW.

| | λ(nm) | ENERGY ($cm^{-1}$) | $A_{JJ'}(S^{-1})$ | $\beta_{JJ'}(\%)$ | $\tau_{\mathrm{rad}}(\mu s)$ |
|---|---|---|---|---|---|
| $^1D_2\rightarrow{}^1G_4$ | 1454,7 | 6874 | 165.082 | 0.79 | 48 |
| $^3F_2$ | 778,6 | 12844 | 920.758 | 4.41 | |
| $^3F_3$ | 747,1 | 13385 | 886.664 | 4.25 | |
| $^3H_4$ | 657,4 | 15212 | 4148.532 | 19.89 | |
| $^3H_5$ | 512,6 | 19508 | 82.949 | 0.39 | |
| $^3F_4$ | 453,1 | 22068 | 4305.884 | 20.65 | |
| $^3H_6$ | 357,7 | 27956 | 10340 | 49.59 | |
| $^1G_4\rightarrow{}^3F_2$ | 1675,0 | 5970 | 11.883 | 047 | 401 |
| $^3F_3$ | 1535,9 | 6511 | 36.134 | 1.44 | |
| $^3H_4$ | 1199,3 | 8338 | 19.281 | 0.77 | |
| $^3H_5$ | 791,5 | 12634 | 461.023 | 18.48 | |
| $^3F_4$ | 658,1 | 15194 | 968.647 | 38.83 | |
| $^3H_6$ | 474,3 | 21082 | 997.387 | 39.98 | |
| $^3F_2\rightarrow{}^3F_3$ | 18484,3 | 541 | 0.012 | 0 | 840 |
| $^3H_4$ | 4223.0 | 2368 | 8.22 | 0.69 | |
| $^3H_5$ | 1500,6 | 6664 | 166.419 | 13.97 | |
| $^3F_4$ | 1084,1 | 9224 | 562.072 | 47.2 | |
| $^3H_6$ | 661,7 | 15112 | 454.09 | 38.13 | |
| $^3F_3\rightarrow{}^3H_4$ | 5473,4 | 1827 | 0.358 | 0.01 | 455 |
| $^3H_5$ | 1633,2 | 6123 | 237.879 | 10.83 | |
| $^3F_4$ | 1151,7 | 8683 | 287.895 | 13.11 | |
| $^3H_6$ | 686,3 | 14571 | 1669.732 | 76.03 | |
| $^3H_4\rightarrow{}^3H_5$ | 2327,7 | 4296 | 30.896 | 1.39 | 451 |
| $^3F_4$ | 1458,6 | 6856 | 82.583 | 3.72 | |
| $^3H_6$ | 784,7 | 12744 | 2101.917 | 94.17 | |
| $^3H_5\rightarrow{}^3F_4$ | 3906,2 | 2560 | 3.718 | 1.82 | 4917 |
| $^3H_6$ | 1183,7 | 8448 | 199.641 | 98.17 | |
| $^3F_4\rightarrow{}^3H_6$ | 1698,4 | 5888 | 95.428 | 100 | 10479 |

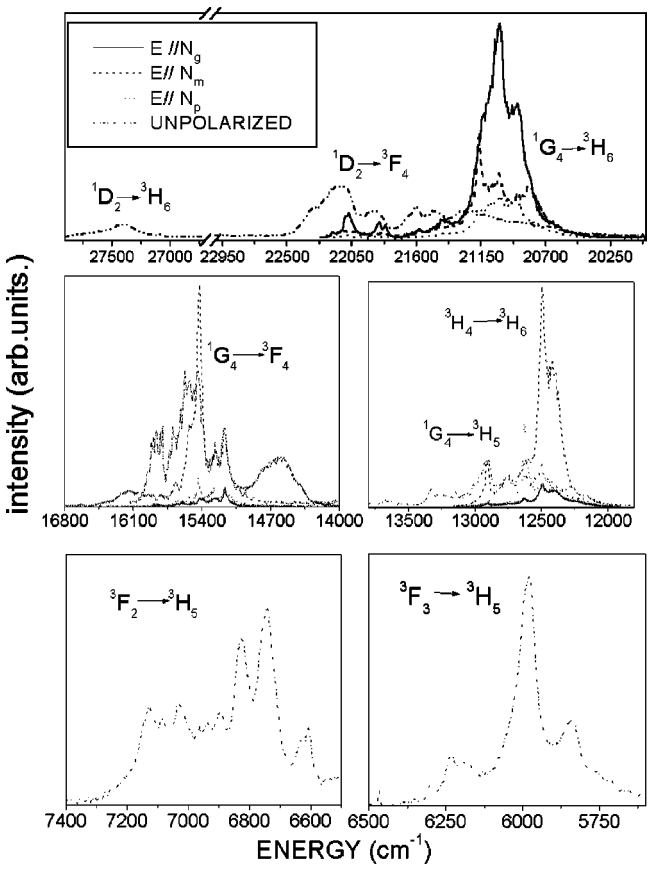


FIG. 5. Room-temperature optical emission of KYbW:Tm.

ests energy sublevels of the ground energy level and the excited energy level. In our case the ratio $Z_l/Z_u$ was 1.27 and $E_{zl}$ was 5564 $cm^{-1}$. Figure 7(b) shows the emission cross section.

As a first approximation, light amplification is expected when the emitted light counterbalances the absorption losses. If $P$ is the population fraction of the excited energy level, this condition can be described as $\sigma_{\text{eff}}=P\sigma_{\text{EM}}-(1-\text{P})\sigma_{\text{GSA}}$, where $\sigma_{\text{eff}}$ is the effective emission cross section, $\sigma_{\text{EM}}$ is the calculated emission cross section and $\sigma_{\text{GSA}}$ is the absorption cross section. Figure 7(a) shows this condition for several polarization configurations in the 1.8–2 $\mu$m spectral region. Figure 8 shows the energy level diagram of $Yb^{3+}$ and $Tm^{3+}$ ions and the emission in the KYbW host.

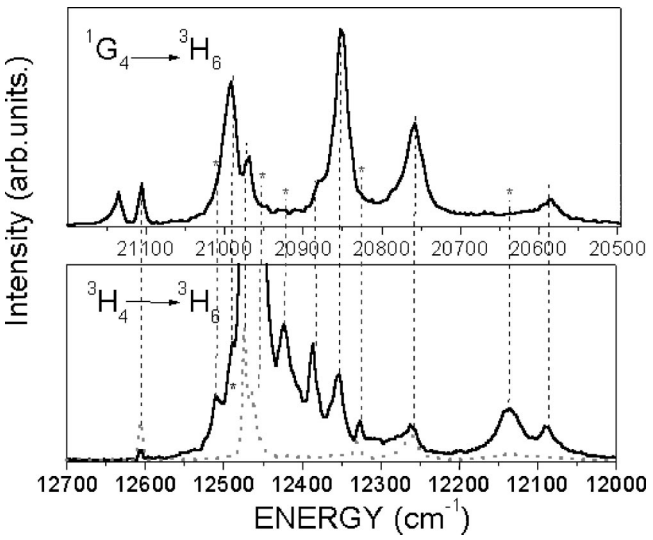


FIG. 6. Low-temperature emission spectra.

### A. Lifetime measurements

We investigated the fluorescence dynamics of the emitting levels as a function of $Tm^{3+}$ concentration at 300 K. The theoretical interpretation of electronic energy transfer phenomena was described in the classical Förster-Dexter model, which describes the resonant interaction between pairs of spatially localized ions via electrostatic multipolar or exchange interactions. Miyakawa and Dexter,[23] and Orbach extended the Förster-Dexter model to systems with nonresonant energy transfer involving phonon absorption or emission. Energy transfer between ytterbium and thulium is via nonresonant energy transfer.

The concentration quenching of lanthanide ion fluorescence in stoichiometric materials shows that linear dependence appears in the non-resonant cross relaxation. The phonon-assisted energy transfer (PAET) was discussed theoretically by Strek.[24] Because of the boson algebra properties of the phonon system, the rate constant is the sum of the squares of all partial acceptor contributions arising from donor-acceptor interactions, so PAET is an incoherent process. In a resonant system the rate constant is given by the square of the sum of all the partial contributions.

We used the above equipment to pump the samples at 10 204 $cm^{-1}$ (980 nm). We analyzed decay time using the

TABLE VI. Emission channels observed in KYbW: $Tm^{3+}$ after pumping at 970 nm.

| | $^{2S+1}L_J \rightarrow {}^{2S'+1}L'_{J'}$ | Energy | wavelength |
|---|---|---|---|
| **i** | $^1D_2 \rightarrow {}^3H_6$ | $E \cong 27900–27000$ $cm^{-1}$ | $\lambda \cong 355–370$ nm |
| **ii** | $^1D_2 \rightarrow {}^3F_4$ | $E \cong 22500–21625$ $cm^{-1}$ | $\lambda \cong 445–463$ nm |
| **iii** | $^1G_4 \rightarrow {}^3H_6$ | $E \cong 21140–20580$ $cm^{-1}$ | $\lambda \cong 473–490$ nm |
| **iv** | $^1G_4 \rightarrow {}^3F_4$ | $E \cong 16000–15000$ $cm^{-1}$ | $\lambda \cong 625–670$ nm |
| **v** | $^1G_4 \rightarrow {}^3H_5$ | $E \cong 13600–12650$ $cm^{-1}$ | $\lambda \cong 735–790$ nm |
| **vi** | $^3H_4 \rightarrow {}^3H_6$ | $E \cong 12650–12000$ $cm^{-1}$ | $\lambda \cong 790–830$ nm |
| **vii** | $^3H_4 \rightarrow {}^3F_4$ | $E \cong 7200–6870$ $cm^{-1}$ | $\lambda \cong 1.39–1.45$ $\mu$m |
| **viii** | $^3F_2 + {}^3F_3 \rightarrow {}^3H_5$ | $E \cong 6870–6580$ $cm^{-1}$ | $\lambda \cong 1.45–1.52$ $\mu$m |
| **ix** | $^3F_4 \rightarrow {}^3H_6$ | $E \cong 5900–5000$ $cm^{-1}$ | $\lambda \cong 1.70–2.0$ $\mu$m |

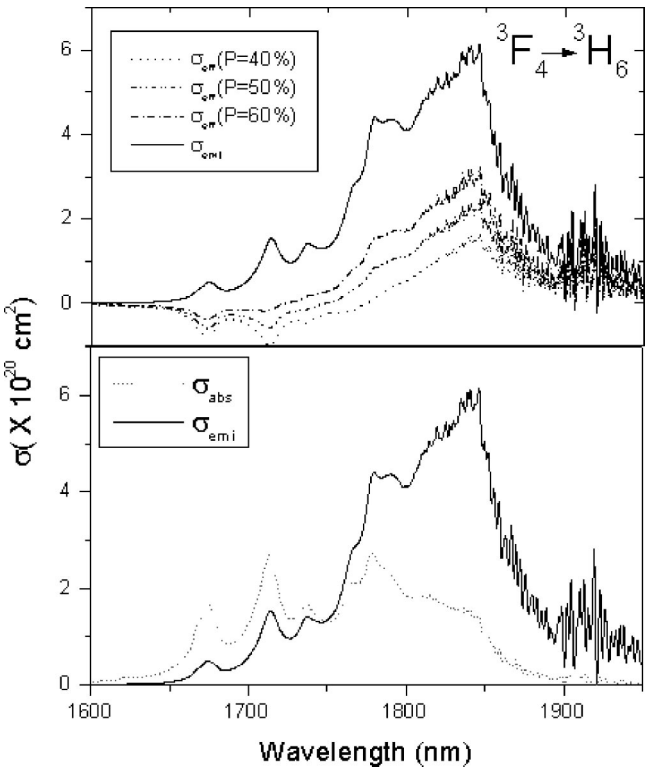


FIG. 7. Emission cross section of KYbW:Tm at room temperature.

averaging facilities of a Lecroy digital oscilloscope. This excited the electrons to the $^2F_{5/2}$ ytterbium excited level via a narrow linewidth BMI VEGA optical parametric oscillator pumped by the third harmonic YAG:Nd laser. We analyzed the emission intensity with an Oriel Monochromator and Hamamatsu PMT in the visible region. We also analyzed the temporal evolution of the up-conversion emissions. The manifold $^2F_{5/2}$ transferred energy to the thulium manifolds.

We studied the room temperature experimental decay of the $^1G_4$ multiplet by measuring $^1G_4 \rightarrow {}^3H_6$ transition at 21 008 cm$^{-1}$ and $^1G_4 \rightarrow {}^3F_3$ transition. The light decay is fitted in both cases by an exponential rise time and an exponential decay time. The rise time was around 30 $\mu$s and the decay time was around 60–70 $\mu$s. The decay time was shorter than the Judd-Ofelt value (406 $\mu$s), which suggests that the decay of the $^1G_4$ level is affected by nonradiative processes. Figure 9 show this evolution in relation to thulium concentration. We can see that rise time and decay time both decreases when the thulium concentration increases. The same behavior was observed in the luminescence decay of the manifolds $^3H_4$.

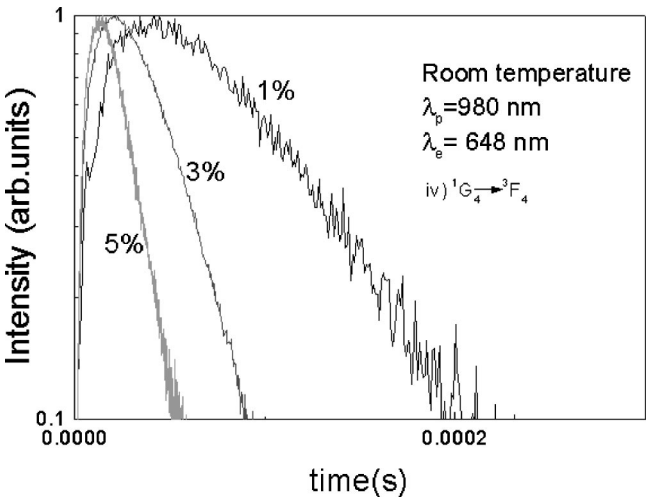


FIG. 9. Lifetime decay of $^1G_4$ manifold at room temperature.

On the other hand, the lifetime of the manifold $^3F_4$ in relation to the increase in thulium concentration behaved strangely (see Fig. 10). This could have been caused by one of two different mechanisms. The first one is a reabsorption effect, which was strong in the emission channels in which $\beta = 1$. The mechanism involved is fluorescence reabsorption, the so-called self-trapping process between $^3F_4 \rightarrow {}^3H_6$ resonant transitions that produces radiative energy transfer between $Tm^{3+}$ ions. This has been mentioned recently in rare-earth-doped crystals such as $Yb^{3+}$-doped $Y_2O_3$.[25] The second mechanism is a repopulation of the emitting manifold via the $^3H_4, {}^3H_6 \rightarrow {}^3F_4, {}^3F_4$ cross-relaxation mechanism that is usually involved. In KYbW, this transfer must be

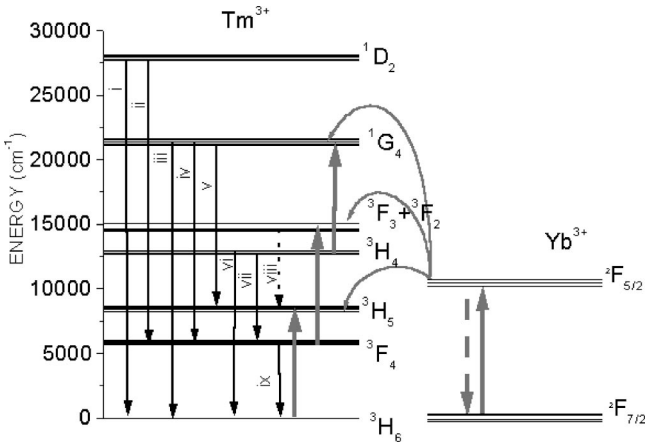


FIG. 8. Diagram of energy levels and emission channels in KYbW:Tm.

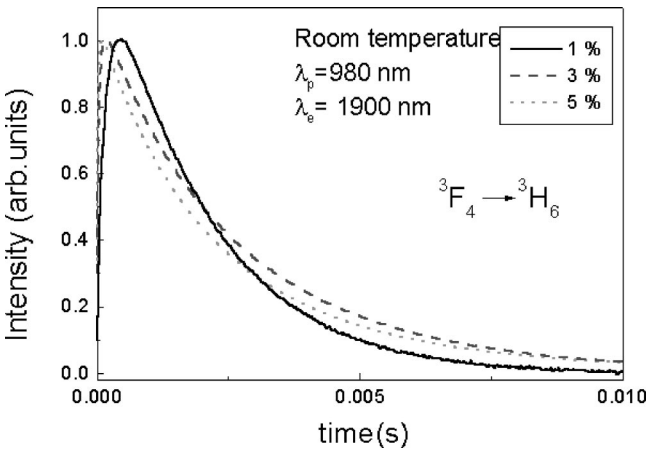


FIG. 10. Lifetime decay of $^3F_4$ manifold at room temperature.

TABLE VII. Experimental lifetimes of the radiative levels of $Tm^{3+}$ in the host KYbW.

| % Tm | $\tau(^1G_4)(\mu s)$ | $\tau(^3H_4)(\mu s)$ | $\tau(^3F_4)(\mu s)$ |
|---|---|---|---|
| 1% | 65 | 90 | 199 |
| 3% | 25 | 30 | 261 |
| 5% | 10 | 9 | 278 |

phonon-assisted since the energy gaps $^3H_6-{}^3F_4=5928\ cm^{-1}$ and $^3H_4-{}^3F_4=6860\ cm^{-1}$ are slightly different.

In summary, in all the visible emissions lifetimes decrease if the concentration increases. The rise time of the decay in luminescence is also high in all cases. This rise time also decreases if the concentration increases. Table VII shows the values of the lifetimes we studied.

## V. CONCLUSIONS

In conclusion, we have performed the crystal growth of $Tm^{3+}$-containing KYbW single crystals with high crystalline quality. We did the spectroscopic characterization of the thulium ion in this host in terms of optical absorption and luminescence. We measured the polarized optical absorption of thulium from the room-temperature and low-temperature experiments to determine the energy position of the excited energy levels of thulium and its splitting due to the crystal field, respectively. We obtained the Judd-Ofelt calculations from optical absorption measurements. We studied the luminescence of thulium in our host from the emission spectra and the lifetime measurement of the main transitions by pumping resonantly to the ytterbium ion (980 nm). We studied the emission spectra for the 480, 800, and 1900 nm emissions to determine the splitting of the ground state and the emission cross section of the 1900 nm emission ($6\times10^{-20}\ cm^2$). Our promising results encourage us to continue researching the laser action of thulium for these emissions.

## ACKNOWLEDGMENTS

This work was supported by CICyT under Project Nos. MAT99-1077-C02, 2FD97-0912-C02, and by CIRIT under Project No. 1999SGR 00183. We also acknowledge financial support from MONOCROM S.L. We gratefully acknowledge S.C.T. of the University of Barcelona (U.B.) for the EPMA measurements.

*Author to whom correspondence should be addressed.

[1] W. Ryba Romanowski, S. Golab, I. Sokolska, G. Dominiak Dzik, J. Zawadzka, M. Berkowski, J. Fink Finowicki, and M. i Baba, Appl. Phys. B: Lasers Opt. **68**, 199 (1999).
[2] B.M. Antipenko, A.A. Mak, O.B. Raba, K.B. Seiranyan, and T.V. Uvarova, Sov. J. Quantum Electron. **12**, 558 (1983).
[3] F. Heine, V. Ostroumov, E. Heumann, T. Jensen, G. Huber, and B.H.T. Chai, OSA Proc. Adv. Solid-State Lasers **24**, 77 (1995).
[4] T. Tomukai, T. Yamamoto, T. Sugawa, and Y. Miyajima, IEEE J. Quantum Electron. **31**, 1880 (1995).
[5] A. Braud, S. Girard, J.L. Doualan, and R. Moncorge, IEEE J. Quantum Electron. **34**, 2246 (1998).
[6] G.J. Kintz, R. Allen, and L. Esterowitz, in Technical Digest, *Conference on Lasers and Electro-Optics* (Optical Society of America, Washington, D.C., 1988), paper FB-2.
[7] A.A. Kaminskii, L. Li, A.V. Butashin, V.S. Mironov, A.A. Pavlyuk, S.N. Bagayev, and K. Ueda, Opt. Rev. **4**, 309 (1997).
[8] A.A. Kaminskii, L. Li, A.V. Butashin, V.S. Mironov, A.A. Pavlyuk, S. N. Bagayev, and K. Ueda, Jpn. J. Appl. Phys., Part 2 **36**, L107 (1997).
[9] S.N. Bagaev, S.M. Vatnik, A.P. Maiorov, A.A. Pavlyuk, and D.V. Plakushchev, IEEE J. Quantum Electron. **30**, 310 (2000).
[10] F.J. McAlaevey, B.D. MacCraith, J. O'Gorman, and J. Hegarty, Fiber Integr. Opt. **16**, 355 (1997).
[11] J.A. Caird, L.G. DeShazer, and J. Nella, IEEE J. Quantum Electron. **11**, 874 (1992).
[12] B.R. Judd, Phys. Rev. **127**, 750 (1962).
[13] G.S. Ofelt, J. Chem. Phys. **37**, 511 (1962).
[14] M.C. Pujol, R. Solé, V. Nikolov, Jna. Gavaldà, J. Massons, C. Zaldo, M. Aguiló, and F. Díaz, J. Mater. Res. **14**, 3739 (1999).
[15] M.C. Pujol, X. Mateos, R. Solé, J. Massons, Jna. Gavaldà, X. Solans, F. Díaz, and M. Aguiló, J. Appl. Crystallogr. **35**, 108 (2001).
[16] M.C. Pujol, M.A. Bursukova, F. Güell, X. Mateos, R. Solé, Jna. Gavaldà, M. Aguiló, J. Massons, F. Diaz, P. Klopp, U. Griebner, and V. Petrov, Phys. Rev. B **65**, 165121 (2002).
[17] J.B. Gruber, M.E. Hills, R.M. Macfarlane, C.A. Morrisson, G.A. Turner, G.L. Quarles, G.J. Kintz, and L. Esterowitz, Phys. Rev. B **40**, 9464 (1989).
[18] C. Li, R. Moncorge, J.C. Souriau, and C. Wyon, Opt. Commun. **101**, 356 (1993).
[19] A.A. Kaminskii, *Crystalline Lasers, Physical Processes and Operating Schemes* (CRC Press, Boca Raton, 1996).
[20] Chr.P. Wyss, M. Kehrli, Th. Huber, P.J. Morris, W. Lüthy, H.P. Weber, A.I. Zagumennyi, Yu.D. Zavartsev, P.A. Studenikin, I.A. Shcherbakov, and A.F. Zerrouk, J. Lumin. **82**, 137 (1999).
[21] B.M. Antipenko, S.P. Vornin, and T.A. Privalova, Opt. Spectrosc. **68**, 164 (1990).
[22] D.E. McCumber, Phys. Rev. A **136**, 954 (1964).
[23] T. Miyakawa and D.L. Dexter, Phys. Rev. B **1**, 2961 (1970).
[24] W. Strek, Phys. Rev. B **29**, 6957 (1984).
[25] L. Laversenne, C. Goutaudier, Y. Guyot, M. Th. Cohen-Adad, and G. Boulon, J. Alloys Compd. (to be published).